journal

J. Am. Ceram. Soc., 86 [1] 115–20 (2003)

Slow-Crack-Growth Behavior of Zirconia-Toughened Alumina Ceramics Processed by Different Methods

Antonio H. De Aza,† Jérôme Chevalier, and Gilbert Fantozzi

INSA—GEMPPM, UMR CNRS 5510, 69621 Villeurbanne, France

Martin Schehl and Ramón Torrecillas*

INCAR, Spanish Research Council (CSIC), 33080 Oviedo, Spain

A study of slow-crack propagation in zirconia-toughened alumina (ZTA) ceramics is presented. Different ZTA composites, using either unstabilized or yttria-stabilized zirconia, have been tested. The materials were prepared in the range 0–15 vol% ZrO_2, using two processing methods: powder mixing and a modified colloidal route. Crack propagation tests have been conducted for crack velocities from 10^{-12} to 10^{-2} m/s by means of a double-torsion method. The influence of the processing conditions and compositions on the microstructures and the effect of these microstructures on the slow-crack-growth behavior have been studied. The option that these composites may offer in terms of the lifetime of ceramic joint prostheses is discussed.

I. Introduction

With the publication of the article "Ceramic Steel?" by Garvie *et al.*,[1] it was shown that the fracture toughness of partially stabilized zirconia materials (PSZ) could be increased by stress-induced martensitic transformation of tetragonal zirconia particles (t-ZrO_2) to the monoclinic form (m-ZrO_2). The incorporation of zirconia (ZrO_2) inclusions into oxide ceramics, especially into alumina matrixes, to deliberately toughen them was undertaken shortly thereafter.[2] The mechanisms by which zirconia acts to toughen the composites are complementary:[3–7] they include transformation toughening, microcracking, and deflection. ZTA composites with high transformation toughening can be obtained if a high portion of tetragonal phase with the ability to transform under applied stress is retained at room temperature. To meet this requirement, the zirconia particles must have a size distribution ranging between the "critical" size for spontaneous transformation on cooling to room temperature after sintering, D_C, and the "critical" size for stress-induced transformation, D'_C. The practical implications in terms of particle size, size distribution, shape, composition, and temperature on the stability of the particles have been outlined by Claussen *et al.*[8] and Garvie.[9] The critical size of ZrO_2 particles for transformation to m-ZrO_2 has been the subject of a number of studies.[3–5,7–16] D_C size is reported to be in the range of 0.5–0.8 μm for unstabilized zirconia in an alumina ceramic matrix[14,15], and $D'_C \approx 0.1$ μm.[16] Processing is thus critical to obtain ZTA ceramics composites with maximum fracture toughness.[17] Today, there is a trend to develop more complex fabrication techniques[14–26] than traditional milling–mixing techniques. They include sol–gel[15,16,21] or colloidal processing,[22] which may allow the obtaining of a narrow size distribution of zirconia particles homogeneously dispersed in the alumina matrix. The addition of Y_2O_3 to ZrO_2 is another possibility to increase the stability of the t-ZrO_2 phase in ZTA systems.[3,4,18–20]

Although slow-crack-growth (SCG) resistance is a critical issue when considering the long-term behavior of ceramic materials, there is only a sparse collection of data in the literature concerning ZTA. It has been observed, in ZTA composites processed from a conventional route, that increasing the contribution of the ZrO_2 phase transformation not only increased the fracture toughness (K_{IC}) but also the required stress to induce crack propagation at a given rate.[19,27] However, little attention has been paid to the threshold (K_{I0}) in the stress-intensity factor under which no crack propagation occurs. This threshold determines a safety range of use for structural applications. The aim of this paper is to study SCG behavior as a function of the processing method and composition in ZTA. In the present investigation, ZTA composites were processed either by a classical route or a modified colloidal method to show the benefit of the latter method on SCG resistance. The overall SCG behavior, including the threshold, of the best ZTA composite processed in this research is measured. It is compared with that of other structural ceramics to keep in mind the option that these materials may offer to improve the lifetime of ceramic joint prostheses.[28]

II. Experimental Procedure

(1) Materials Processing

ZTA composites were prepared in the range of 0 vol% ZrO_2 (pure alumina) to 15 vol% ZrO_2. They were processed either by a conventional powder-mixing processing route or by a modified colloidal processing route.

Concerning the conventional powder-mixing technique, a high-purity alumina powder, α-Al_2O_3 > 99.9 wt% (HPA-0.5, Ceralox Division, Condea Vista Co., Tucson, AZ) with an average particle size of 0.49 μm and a specific surface area of 10 m^2/g (values given by the supplier), was used to process pure alumina samples. Stable suspensions, pH ≈ 4 in water media, of this alumina powder were homogeneously mixed with different amounts (10 and 15 vol%) of a (>99.9 wt% purity) monoclinic zirconia powder (TZ 0, Tosoh Corp., Tokyo, Japan) with a mean particle diameter of 0.47 μm and a specific surface area of 15.5 m^2/g (values given by the supplier). To homogenize, the batches were wet ground in a laboratory-scale annular gap mill[29] with high-purity alumina balls of 3 mm diameter, after which they were spray-dried. Quantitative X-ray diffraction (XRD) (Model D5000-Kristalloflex 710, Siemens, Karlsruhe, Germany) was performed to ensure that there was no preferential loss or segregation during the spray-drying process. The average particle size of the final batches,

N. Claussen—contributing editor

Manuscript No. 187654. Received June 7, 2001; approved September 5, 2002.

Supported by the Ministry of Education and Culture of Spain (PF9805271356) and MCYT MAT 2000-0941.

*Member, American Ceramic Society.

†Author to whom all correspondence should be addressed. Present address: ICV-CSIC, Campus de Cantoblanco 28049, Cantoblanco (Madrid) Spain, aaza@icv.csic.es

measured by laser diffraction (Model LS 130, Coulter Corp., Miami, FL), was between 0.33–0.4 μm. The specific surface area, measured by a 5-point BET method (Model ASAP 2010, Micromeritics Instrument Corp., Norcross, GA) was 10 ± 2 m^2/g for all batches processed from this classical route. The final particle size and BET-specific surface area are in fair agreement with the values given by the suppliers for the raw materials.

ZTA batches with the same zirconia proportion were also processed through a modified colloidal processing route developed by Schehl *et al.*[30] A composition with 7.5 vol% ZrO_2 was additionally processed. Stable suspensions of the above-mentioned alumina powder in absolute ethanol (99.97%) were doped by dropwise addition of a diluted (2/3 (vol%) zirconium alkoxide solution, 1/3 (vol%) ethanol absolute) zirconium alkoxide solution (zirconium(IV) propoxide 70 wt% solution in 1-propanol, Aldrich Chemical, Milwaukee, WI). The main difference with a standard solution method[15,26,31] using metal alkoxides is that the metal alkoxide is not hydrolized in the suspension. After drying under magnetic stirring at 70°C, the powders were thermally treated at 850°C for 2 h and were subsequently attrition milled, as a suspension in alcohol, with 3 mm alumina balls for 1 h. The powders were then dried and sieved to <45 μm. The specific surface area of the final powders ranged between 10 m^2/g for 7.5 vol% ZrO_2 and 14 m^2/g for 15 vol% ZrO_2 (they were all close to the initial specific surface area of alumina).

A composition with 7.5 vol% ZrO_2, stabilized by 2 mol% Y_2O_3, was additionally processed by the colloidal route described. For this purpose, the batch was also doped by dropwise addition of a diluted (2/3 (vol%) Y alkoxide, 1/3 (vol%) ethanol absolute) yttrium alkoxide (yttrium methoxyethoxide 15%–18% in methoxyethanol, Gelest ABCR GmbH & Co., Karlsruhe, Germany). The measured specific surface area was 10 m^2/g.

Next, all batches were uniaxially pressed at 20 MPa to a rectangular shape in a die (60 mm × 30 mm) to produce green compacts with just enough strength to be moved into an isostatic press, where they were cold isostatically pressed at 200 MPa. The temperature–time sintering conditions were studied by means of dilatometric analysis (Model DI-24, Adamel-Lhomargy Division d' Instruments S.A., Ivry-S/Seine, France). Final composites were sintered in air at 1550°C for 2 h, whereas the pure alumina samples were sintered at 1500°C for 2 h, with the aim of avoiding a high grain-growth rate. The bulk density of the obtained materials was measured by the Archimedes method.

(2) XRD Analysis and Microscopy Observations

The sintered samples were machined (2 mm × 20 mm × 40 mm) and polished with a series of diamond pastes up to 1 μm. XRD data, from unpolished, polished, and fractured surfaces, were obtained with a diffractometer using nickel-filtered Cu*K*α radiation. The tetragonal/monoclinic zirconia ratio was determined using the integrated intensity (measuring the area under the diffractometer peaks) of the tetragonal (101) and two monoclinic ($\bar{1}11$) and (111) peaks as described by Toroya *et al.*[32] For the purposes of comparison, the obtained volume fractions of tetragonal ZrO_2 ($V_t = 100 - V_{m;}$ V_m denotes the volume fraction of monoclinic ZrO_2) were individually normalized to the volume fractions of ZrO_2 (V_{ZrO_2}) present in each composite as follows:

$$\frac{V_t \times V_{ZrO_2}}{100} = V_{t(\text{composite})} \tag{1}$$

Additionally, the transformation of the tetragonal grains to monoclinic symmetry accompanying the propagating crack (ΔV_m) was investigated. This analysis was performed by XRD on the double-torsion sample crack plane after fracture from crack-propagation tests. Although the X-ray penetration is too deep to be considered as a real surface analysis, this test allowed a rough estimate of the stress-induced phase transformation in the materials to be obtained.

The average alumina and zirconia grain sizes were measured using micrographs via scanning electron microscopy (SEM; Model XL20, Philips, Eindhoven, The Netherlands) of polished and thermally etched surfaces using a linear intercept method (ASTM standard test method E112, American Society for Testing and Materials, West Conshohocken, PA) and using an image analyzer program (Scion Image, Scion Corp., Frederick, MD) where the diameter (d) was calculated from the projected particle area (A) using the well-known stereological expression:

$$d = 2\left(\frac{A}{\pi}\right)^{1/2} \tag{2}$$

(3) Crack-Growth Measurements

The double-torsion (DT) method was used to obtain the V–K_I (crack velocity versus stress-intensity factor) diagrams. The geometry of the DT specimen and the loading configuration can be found elsewhere.[33,34] No guiding groove was machined in the specimens to avoid any residual stress. Both sides of the specimens were polished, but the tensile surface was polished to a 1 μm finish to observe the crack with precision of ±2 μm using reflected-light microscopy (Model HP1, Karl Zeiss, Thornwood, NY). A notch of length $a_0 \approx 10$ mm was machined by a 0.3 mm diamond saw. A small natural crack was then induced in the specimen by slow precracking (loading rate 10 μm/min) up to ~12–13 mm ($\Delta a_0 \approx$ 2–3 mm). For a long time, the DT configuration has been considered to yield a stress-intensity factor independent of crack length. According to the specimen geometry, the conventional expression for K_I is given as:[34]

$$K_I = \frac{W_m}{T^2}\left[\frac{3(1+\nu)}{\psi \cdot W}\right]^{1/2} P = HP \tag{3}$$

with

$$\psi = 1 - 0.6302\left[2\left(\frac{T}{W}\right)\right] + 1.20\left[2\left(\frac{T}{W}\right)\right]\exp\left[\frac{-\pi}{2(T/W)}\right] \tag{4}$$

where P is the applied load, W_m the half-distance between the two points of flexion (moment arm), W the width, T the thickness of the specimen, and ν is the Poisson ratio.

However, it has been recently demonstrated that K_I was slightly dependent on the crack length,[35,36] and to obtain accurate V–K_I diagrams, a correction factor[35] should be introduced in the conventional expression of K_I (Eq. (3)). This correction is expressed with the following empirical equation:

$$K_{ICorr} = HP\left(\frac{a}{a_0}\right)^{6/32} \tag{5}$$

where a_0 is the notch length and a is the total crack length.

Subcritical-crack-growth laws were determined via two methods: relaxation tests and constant-loading tests. The load-relaxation method, which was first reported by Williams and Evans,[34] was used to obtain the SCG V–K_I diagrams in the velocity range 10^{-2}–10^{-7} m/s. This method does not allow measurements at very low velocity; however, it does present the advantage of being fast and, in principle, a full curve can be recorded in a single experiment. Precracked specimens were loaded at a constant rate of 0.2 mm/min, followed by subsequent stopping of the crosshead at constant displacement, when the crack started to propagate. The obtained load-relaxation versus time (P vs t) plot allows the determination of the V–K_I curve by a compliance calibration.[34,35] More details concerning the method for determination of V–K_I curves from P–t plots can be found elsewhere.[33–39]

Measurement of the crack velocities (V) under constant load presents the advantage of allowing the measurement of very low velocities. Thus, the specimens were subjected to different static loads under a prescribed duration, Δt. The crack length was

Table I. Designation and Main Characteristics of the Tested Materials

Ceramic material	Powder specific surface area (m^2/g)	Sintering conditions	% Theoretical density	Al_2O_3 grain size (μm)	ZrO_2 grain size (μm)	K_{IC} ($MPa \cdot m^{1/2}$) DT	Volume fraction (V_m) of monoclinic ZrO_2 after sintering	Stress-induced monoclinic content (ΔV_m %)	Designation
Alumina	10 ± 1.5	1500°C/2 h (air)	98.5	1.7		4.2 ± 0.2			Al_2O_3
Powder processing									
Al_2O_3–10 vol% ZrO_2		1500°C/2 h (air)	98	1.7	0.7	5.4 ± 0.2	45 ± 2	27	$A10Z^{Pw}$
Al_2O_3–15 vol% ZrO_2	11 ± 1.5	1550°C/2 h (air)	98	1.7	0.7	4.5 ± 0.2	81 ± 4	0	$A15Z^{Pw}$
Colloidal processing									
Al_2O_3–7.5 vol% ZrO_2	10 ± 1.5	1550°C/2 h (air)	98	1.2	0.4	5.5 ± 0.2	22 ± 1	21	A7.5Z
Al_2O_3–10 vol% ZrO_2	12 ± 1.5	1550°C/2 h (air)	98	1.2	0.4	5.9 ± 0.2	40 ± 2	29	A10Z
Al_2O_3–15 vol% ZrO_2	14 ± 1.5	1550°C/2 h (air)	98	1.2	0.4	5 ± 0.2	78 ± 4	0.5	A15Z
Al_2O_3–7.5 vol% ZrO_2 with 2 mol% Y_2O_3	10 ± 1.5	1550°C/2 h (air)	98	1.1	0.4	5.3 ± 0.2	19 ± 1	7	A7.5Z-2Y

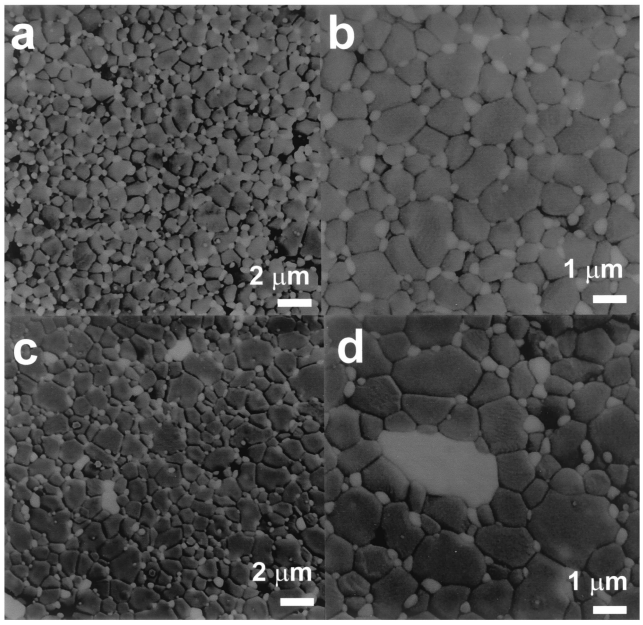

Fig. 1. Backscattered SEM images showing the microstructure of the Al_2O_3–10-vol%-ZrO_2 composites obtained. Samples show ZrO_2 grains (the brighter phase) distributed in a fine-grain Al_2O_3 matrix (the darker phase). (a) and (b): Nanocomposite processed by the colloidal processing route described (Al_2O_3 D_{50} = 1.2 ± 0.4 μm and ZrO_2 D_{50} = 0.4 ± 0.1 μm); (c) and (d): Composite processed by the conventional powder-mixing processing technique (Al_2O_3 D_{50} = 1.7 ± 0.6 μm and ZrO_2 D_{50} = 0.7 ± 0.4 μm).

measured via optical microscopy, with a precision of ±2 μm, and V is defined as the ratio of crack increment, Δa, to the duration, Δt:

$$V = \frac{\Delta a}{\Delta t} \tag{6}$$

From the obtained data, the threshold (K_{I0}) value was determined by extrapolation from the points on the V–K_I diagram, below which there is an abrupt drop of the crack velocity. On the other hand, the toughness (K_{IC}) was determined by extrapolation of the V–K_I curve to high-crack velocities (10^{-2} m/s).

III. Results and Discussion

The designation and main characteristics of each material are summarized in Table I.

Figures 1(a)–(d) show the final microstructures of the Al_2O_3–

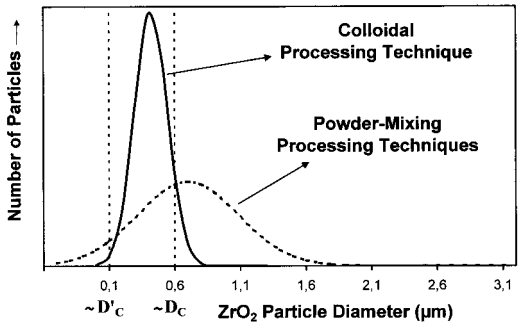

Fig. 2. ZrO_2 grain-size distribution in the alumina–10-vol%-zirconia composites obtained by conventional powder-mixing processing technique and a colloidal processing route (assuming a normal distribution of zirconia particle sizes). The values given for D_C and D'_C are reported values[14–16] for unstabilized zirconia in Al_2O_3–ZrO_2 composites.

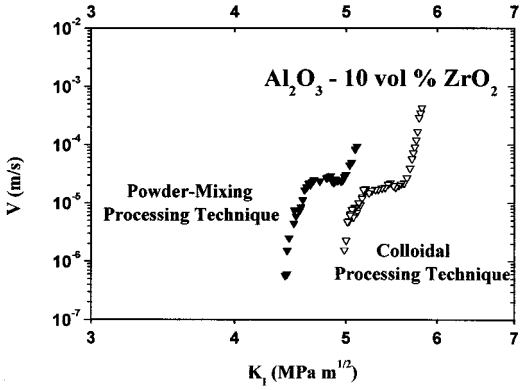

Fig. 3. Crack velocity (V) versus stress-intensity factor (K_I) for the alumina 10 vol% zirconia composites obtained by conventional powder-mixing processing technique and the colloidal processing route described; the finer microstructure obtained by colloidal processing leads to a displacement of the V–K_I diagram to higher K_I values.

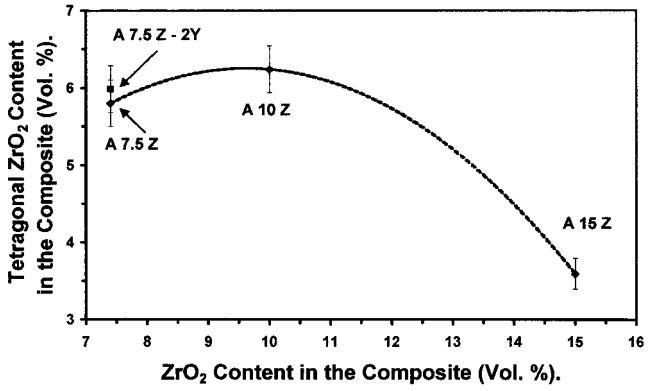

Fig. 5. Tetragonal zirconia retained after sintering in the ZTA composite ($V_{t(composite)} = (V_t V_{ZrO_2})/100$), as a function of zirconia content in the composite. Data from unpolished surfaces.

10-vol%-ZrO_2 composites obtained either by the powder-mixing processing technique or the colloidal processing route described. The figures show ZrO_2 grains (the brighter phase) distributed in an Al_2O_3 matrix (the darker phase). The composite obtained by the colloidal processing route (Figs. 1(a) and (b)) show nano-sized ZrO_2 particles ($D_{50} = 0.4 \pm 0{,}1$ μm) homogeneously distributed at Al_2O_3 grain boundaries ($D_{50} = 1.2 \pm 0.4$ μm), without agglomerates and a minimum number of microstructural flaws. The composite obtained by the conventional powder-mixing technique (Figs. 1(c) and (d)) show larger ZrO_2 particles ($D_{50} = 0.7 \pm 0.4$ μm) less homogeneously distributed in the Al_2O_3 matrix. Al_2O_3 also exhibits larger grains ($D_{50} = 1.7 \pm 0.6$ μm). Figure 2 compares the ZrO_2 grain-size distributions of the two A10Z composites, assuming a normal distribution of zirconia particle sizes. It is shown that the alumina zirconia composite processed by colloidal method has a narrow size distribution that is roughly between the critical size for spontaneous transformation on cooling to room temperature (D_C) and the critical size for stress-induced transformation (D'_C).[14–16] The above-mentioned fact leads to a more efficient transformation toughening in the material processed by the colloidal route. In this material, a transformation of the tetragonal grains toward monoclinic symmetry ahead of a propagating crack (ΔV_m) ~12% higher than for the composite processed by the conventional powder-mixing technique was found, highlighting higher transformability. As mentioned in the previous section, this analysis was performed by XRD on the DT crack plane after fracture from crack-propagation tests and gives a rough estimate of the stress-induced phase transformation in both materials. This more efficient transformation toughening leads to a shift of the obtained V–K_I diagrams toward higher K_I values for the composites processed by the colloidal route when compared with the same compositions processed by the powder-mixing technique. Figure 3 highlights this fact that is reflected in a higher crack growth resistance of the composite A10Z obtained by the colloidal processing route. This behavior was confirmed for all the compositions.

As the composites processed by the colloidal route exhibit better mechanical properties than those processed by the powder-mixing technique, from now on, the results and discussion will be focused on this type of composite.

The measured V–K_I diagrams of alumina and the composites, prepared with different volume fraction of unstabilized zirconia, are plotted in Fig. 4. The curves exhibit a trend to shift toward higher K_I values up to a maximum before dropping with increasing volume fraction. These results are in agreement with previously reported values on the toughness of Al_2O_3–ZrO_2 composites.[2,27] The increasing crack resistance of the composites can be explained by the transformation mechanism mentioned. The tetragonal ZrO_2 concentration in the ZTA composites ($V_{t(composite)}$) after sintering, plotted in Fig. 5, is calculated from Eq. (1) and from the values of monoclinic content measured by XRD that are shown in Table I. The A10Z composite is the one with the highest amount of tetragonal phase retained at room temperature in the whole composite. Additionally, Fig. 6 shows the stress-induced phase transformation of the metastable tetragonal grains toward monoclinic symmetry ahead of a propagating crack (ΔV_m%). The term ΔV_m% corresponds to the difference in percent between monoclinic content measured on fractured and sintered surface (Table I) and gives estimate of transformation toughening efficiency. Here,

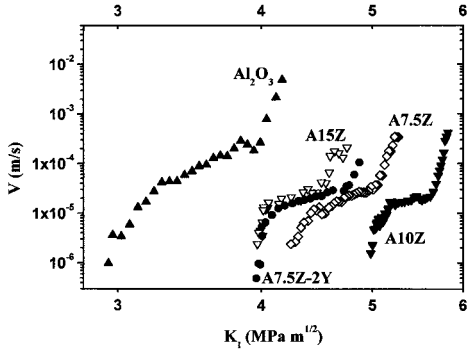

Fig. 4. Crack velocity (V) versus stress-intensity factor (K_I) diagrams for Al_2O_3 and the A7.5Z, A10Z, A15Z, and A7.5Z-2Y composites processed by the colloidal technique described.

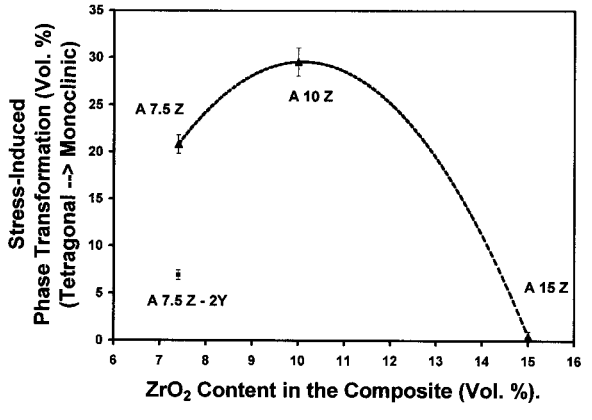

Fig. 6. Stress-induced phase transformation of the metastable tetragonal grains to monoclinic symmetry (ΔV_m%), measured on the fracture surface for colloidal processed series.

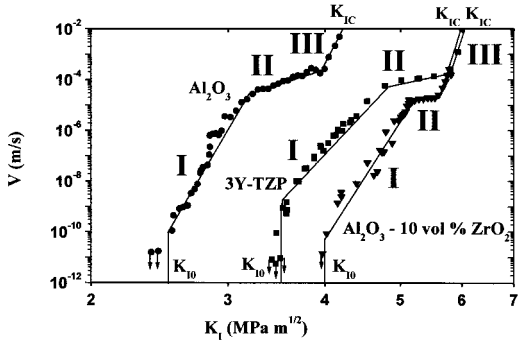

Fig. 7. Crack velocity (V) versus the stress-intensity factor (K_I) for Al_2O_3, Al_2O_3–10-vol%-ZrO_2 composite and 3Y-TZP;[40,41] the alumina–zirconia composite processed via the mentioned colloidal processing route exhibits the highest slow crack growth resistance. ((●) Al_2O_3, (▼) A10Z, and (■) 3Y-TZP.) Arrows indicate tests where no propagation could be observed, crack rate must be lower than the value plotted.

it can be seen that the A10Z composite has the highest effective transformation and the A15Z the lowest. As indicated by Claussen,[2] the amount of stress in the matrix increases with the amount of zirconia dispersed, and, beyond a maximum, the matrix is not able to retain the tetragonal ZrO_2 as a metastable phase. Additionally, it is worth noting that the critical ZrO_2 particle size for transformation is dependent on the volume fraction of ZrO_2 present in the matrix, as reported by Green.[5] For high-volume fractions of ZrO_2, the volume expansion (3%–5%) caused by the transformation leads to a high density of microcracks, which join up between the transformed particles. Consequently, the K_{IC} value decreases and the overall V--K_I curve is shifted toward lower K_I values.

Next, Fig. 4 also shows the measured V–K_I diagram of the A7.5Z composite processed with 2 mol% of Y_2O_3 (A7.5Z-2Y). The V–K_I curve of the composition with yttria is slightly shifted to lower K_I values compared with the batch A7.5Z. The V–K_I curve of this material lines up with the material A15Z. This lower crack resistance corresponds to a lower (if no) effective transformation toughening, as shown in Fig. 6 and Table I. The use of the 2 mol% of Y_2O_3 to stabilize the t-ZrO_2 limits the effectiveness of the transformation-toughening mechanism when an external stress is applied and processing modifications would be required to increase the size and/or the amount of the Y_2O_3-stabilized ZrO_2 particles. Figure 4 and Table I show that composites processed from the colloidal route always exhibit higher crack resistance than pure alumina, even for A15Z and A7.5Z-2Y where little or no transformation occurs. Note that transformation toughening is not the only mechanism acting to reinforce alumina in ZTA, and that complementary processes, i.e., crack deflection and microcracking, occur. These complementary toughening mechanisms already account for the crack resistance of ZTA, because they give an increase of $\sim$1 MPa·m$^{1/2}$ of crack resistance compared with alumina. In any case, the material exhibiting the highest amount of phase transformation during crack extension (i.e., A10Z) presents the highest crack resistance.

Finally, the whole crack velocity diagrams of the A10Z composite obtained by the colloidal route and Al_2O_3 are compared in Fig. 7. Additionally, in the same figure, keeping in mind the option that these materials may offer to improve the lifetime of ceramic joint prostheses[28], both curves are compared with other results for a 3Y-TZP (3-mol%-yttria-stabilized zirconia) bioceramic.[40,41]

The overall curves obtained in air exhibits three distinct stages that have been fitted to a power law:[42]

$$V = AK_I^n \tag{7}$$

The different values of parameters A and n are reported in Table II. Thresholds below which no crack propagation occurs (K_{I0}) were observed at values indicated in the table. Figure 7 shows that the zirconia ceramic (3Y-TZP) exhibits a higher toughness than alumina but the thresholds of both materials are lower than that of the alumina–zirconia nanocomposite (also see Table II), meaning that the necessary stress to initiate crack growth is lower in alumina and 3Y-TZP. Additionally, the alumina-zirconia nanocomposite has a toughness close to that of zirconia but a higher threshold, a consequence of the steeper slope of its V–K_I diagram. SCG in ceramics is attributed to stress-assisted corrosion at the crack tip or any pre-existing defect in the ceramic. This is indeed the combined effect of high stresses at the crack tip and the presence of water or environmental species, temperature, and other extraneous variables (reducing surface energy at the crack tip) that induce crack propagation in a subcritical manner.[42] Alumina has lower susceptibility to water and thus to stress-assisted corrosion. As a consequence, the V–K_I curve of alumina presents a higher slope than the curve corresponding to zirconia. From an atomistic point of view, this means that the fracture energy of zirconia is lower in the presence of water, because the zirconia bonds are prone to chemisorption of the polar water molecules. The addition of a small amount of zirconia to alumina (in Fig. 7, 10 vol%) has two main advantages: first, alumina-zirconia composites exhibit crack propagation primarily through the alumina matrix. Thus, these composites possess a low susceptibility to stress-assisted corrosion from water. Second, these materials are reinforced by the presence of highly transformable zirconia particles, shifting the V–K_I diagram of alumina toward higher K_I values while preserving the slope of the curve, as it was theoretically shown previously.[43] Figure 7 and Table II show that the current results are in agreement with this previous work, primarily in the first stage of the curve, where the effect of the stress-assisted corrosion is higher.

In any case, the threshold K_{I0} represents the key parameter as far as durability is concerned[44] (as for orthopedic implants, which must survive *in vivo* for more than 10 years). From the well-known stress-intensity factor equation:

$$K_I = Y\sigma a^{1/2} \tag{8}$$

where Y is a shape factor related to the crack, σ the applied stress, and a the size of a pre-existing defect, it is expected that no failure occurs *in vivo* if the applied stress is lower than

$$\sigma_0 = \frac{K_{I0}}{Ya^{1/2}} \tag{9}$$

The K_{I0} value of the best ZTA composite processed in this research (10 vol% of ZrO_2) is twice that of pure alumina. This means that for the same pre-existing defects, this composite is expected to work at loads two times greater than monolithic alumina without any delayed failure.

Table II. Threshold (K_{I0}), Toughness (K_{IC}), and Slow-Crack-Growth Parameters (A and n) of Al_2O_3, A10Z, and 3Y-TZP Materials†

Material	Threshold (K_{I0}) MPa·m$^{1/2}$	Toughness (K_{IC}) MPa·m$^{1/2}$	1st stage		2nd stage		3rd stage	
			A	n	A	n	A	n
Al_2O_3	2.5 ± 0.2	4.2 ± 0.2	2×10^{-33}	56.8	3×10^{-11}	12	4×10^{-40}	59.7
A10Z	4.0 ± 0.2	5.9 ± 0.2	4×10^{-43}	53.5	5×10^{-9}	4.8	7×10^{-50}	59.6
3Y-TZP‡	3.5 ± 0.2	6.1 ± 0.2	1.8×10^{-26}	31.5	1.4×10^{-9}	6.6	9.3×10^{-53}	64

†Tested in air. ‡Data from Refs. 40 and 41.

IV. Conclusions

The following conclusions can be drawn:

(1) The microstructures of the alumina-zirconia composites obtained by the modified colloidal processing technique are very fine with a narrow distribution of zirconia particles homogeneously dispersed in the alumina matrix. This leads to a high portion of tetragonal phase retained after sintering with the ability to transform under applied stress. These composites show an increase of crack resistance compared with the composites processed with a classical powder-mixing route.

(2) The measured V–K_I diagrams of the composites are shifted toward higher K_I values with increasing transformable ZrO_2 volume fraction, up to ~10%. This trend is inverted at volume fractions beyond a maximum. The use of the 2 mol% of Y_2O_3 to stabilize the t-ZrO_2 could limit the effectiveness of the transformation toughening mechanism for the particle size obtained when an external stress is applied, and it would require processing modifications to increase crack resistance.

(3) The best alumina-zirconia composite developed in this study, A10Z, presents a threshold, K_{I0}, significantly higher than monolithic alumina and zirconia. This should offer the option of improving the safety range of use of orthopedic implants.

Acknowledgments

The authors wish to express their appreciation to L. A. Diaz and to J. L. Rodríguez for his kind help with sample preparations.

References

[1]R. C. Garvie, R. H. J. Hannink, and R. T. Pascoe, "Ceramic Steel?," *Nature (London)*, **258**, 703–704 (1975).

[2]N. Claussen, "Fracture Toughness of Al_2O_3 with an Unstabilized ZrO_2 Dispersed Phase," *J. Am. Ceram. Soc.*, **59** [1–2] 49–51 (1976).

[3]D. J. Green, R. H. J. Hannink, and M. V. Swain, *Transformation Toughening of Ceramics*; p. 232. CRC Press, Boca Raton, FL, 1989.

[4]R. H. J. Hannink, P. M. Kelly, and B. C. Muddle, "Transformation Toughening in Zirconia-Containing Ceramics," *J. Am. Ceram. Soc.*, **83** [3] 461–87 (2000).

[5]D. J. Green, "Critical Microstructures for Microcracking in Al_2O_3-ZrO_2 Composites," *J. Am. Ceram. Soc.*, **65** [12] 610–14 (1982).

[6]N. Claussen, J. Steeb, and R. F. Pabst, "Effect of Induced Microcracking on the Fracture Toughness of Ceramics," *Am. Ceram. Soc. Bull.*, **56** [6] 559–62 (1977).

[7]N. Claussen, "Stress-Induced Transformation of Tetragonal ZrO_2 Particles in Ceramic Matrices," *J. Am. Ceram. Soc.*, **61**, 85 (1978).

[8]N. Claussen and M. Rühle, "Design of Transformation-Toughened Ceramics"; pp. 137–63 in Advances in Ceramics, Vol. 3, *Science and Technology of Zirconia I*. Edited by A. H. Heuer and L. W. Hobbs. American Ceramic Society, Columbus, OH, 1981.

[9]R. C. Garvie, "Critical Size Effects in Alumina-Zirconia Alloys"; pp. 55–69 in Advanced in Ceramics, Vol. 24A, *Science and Technology of Zirconia III*. Edited by S. Sōmiya, N. Yamamoto, and H. Hanagida. American Ceramic Society, Westerville, OH, 1988.

[10]A. H. Heuer, N. Claussen, W. M. Kriven, and M. Rühle, "Stability of Tetragonal ZrO_2 Particles in Ceramic Matrices," *J. Am. Ceram. Soc.*, **65** [12] 642–50 (1982).

[11]F. F. Lange, "Transformation Toughening: Part I, Size Effects Associated with the Thermodynamics of Constrained Transformations," *J. Mater. Sci.*, **17** [1] 225–34 (1982).

[12]F. F. Lange and D. J. Green, "Effects of Inclusion Size on the Retention of Tetragonal ZrO_2: Theory and Experiments"; see Ref. 8, pp. 217–25.

[13]A. H. Heuer, "Stability of Tetragonal ZrO_2 Particles in Ceramic Matrices," *J. Am. Ceram. Soc.*, **65** [12] 642–50 (1982).

[14]G. L. Messing and M. Kumagai, "Low-Temperature Sintering of Seeded Sol–Gel-Derived, ZrO_2-Toughened Al_2O_3 Composites," *J. Am. Ceram. Soc.*, **72** [1] 40–44 (1989).

[15]V. V. Srdic and L. Radonjic, "Transformation Toughening in Sol–Gel-Derived Alumina-Zirconia Composites," *J. Am. Ceram. Soc.*, **80** [8] 2056–60 (1997).

[16]F. Thevenot and P. Homerin, "Composites Alumine-Zircone"; pp. 39–57 in *Ceramiques Composites a Particules, cas du Frittage-Reaction (FORCERAM)*. Edited by F. Thevenot. Septima, Paris, France, 1992.

[17]F. F. Lange, "Powder Processing Science and Technology for Increased Reability," *J. Am. Ceram. Soc.*, **72** [1] 3–15 (1989).

[18]F. F. Lange, "Transformation Toughening: Part 5, Effect of Temperature and Alloy on Fracture Toughness," *J. Mater. Sci.*, **17** [1] 225–62 (1982).

[19]P. F. Becher, "Slow Crack Behavior in Transformation-Toughened Al_2O_3-ZrO_2 (Y_2O_3) Ceramics," *J. Am. Ceram. Soc.*, **66** [7] 485–88 (1983).

[20]K. Tsukuma, K. Ueda, and M. Shimada, "Strength and Fracture Toughness of Hot Isostatic-Pressed Y_2O_3-Partially Stabilized ZrO_2/Al_2O_3 Composites," *J. Am. Ceram. Soc.* **68** [1] C-4 (1985).

[21]P. F. Becher, "Transient Thermal Stress Behavior in ZrO_2-Toughened Al_2O_3," *J. Am. Ceram. Soc.*, **64** [1] 37–39 (1981).

[22]I. A. Aksay, F. F. Lange, and B. I. Davis, "Uniformity of Al_2O_3-ZrO_2 Composites by Colloidal Filtration," *J. Am. Ceram. Soc.*, **66** [10] C-190–C-192 (1983).

[23]S. Hori, M. Yoshimura, and S. Sōmiya, "Al_2O_3–ZrO_2 Ceramics Prepared from CVD Powders"; pp. 794–805 in Advances in Ceramics, Vol. 12, *Science and Technology of Zirconia II*. Edited by N. Claussen, M. Rühle, and A. H. Heuer. American Ceramic Society, Columbus, OH, 1984.

[24]D. W. Sproson and G. L. Messing, "Preparation of Alumina-Zirconia Powders by Evaporative Decomposition Solutions," *J. Am. Ceram. Soc.*, **67** [7] C-92–C-93 (1984).

[25]S. Somiya, S. Kikugawa, and M. Yoshimura, "Fine Grained Al_2O_3-ZrO_2 Ceramics by Hydrothermal Reaction Sintering," *Am. Ceram. Soc. Bull.*, **63** [3] 459 (1984).

[26]B. Fegley Jr., P. White, and H. K. Bowen, "Preparation of Zirconia-Alumina Powders by Zirconium Alkoxide Hydrolysis," *J. Am. Ceram. Soc.*, **68** [2] C-60–C-62 (1985).

[27]G. Fantozzi and G. Orange, "Thermomechanical Properties of Zirconia Toughened Alumina Materials"; pp. 188–215 in *Processing of Advanced Ceramics*. Edited by J. S. Moya and S. De Aza. Societie de Espana Cerámica Vidro. Arganda del Rey, Madrid, Spain, 1986.

[28]J. Chevalier, A. H. De Aza, G. Fantozzi, M. Schehl, and R. Torrecillas, "Extending the Lifetime of Orthopaedic Implants," *Adv. Mater.*, **12** [21] 1619–21 (2000).

[29]W. Cremer, "Defined Grinding in a Grinding Chamber Formed as an Annular Gap," *Interceram*, [5] 59–61 (1989).

[30]M. Schehl, L. A. Díaz, and R. Torrecillas, "Alumina Nanocomposites from Powder-Alkoxide Mixtures," *Acta Mater.*, **50**, 1125–39 (2002).

[31]S. Hirano, T. Yogo, and K. Kikuta, "Processing of Functional Ceramics by Metallorganic Route," *J. Ceram. Soc. Jpn.*, **99** [10] 1026–35 (1991).

[32]H. Toroya, M. Yoshimura, and S. Sōmiya, "Calibrated Curve for Quantitative Analysis of the Monoclinic-Tetragonal ZrO_2 System by X-Ray Diffraction," *J. Am. Ceram. Soc.*, **67** [6] C-119–C-121 (1984).

[33]A. G. Evans, "A Method for Evaluating the Time-Dependent Failure Characteristics of Brittle Materials and Its Application to Polycrystalline Alumina," *J. Mater. Sci.*, **7**, 1137–46 (1972).

[34]D. P. Williams and A. G. Evans, "A Simple Method to Study Slow Crack Growth," *J. Test. Eval.*, **1** [4] 264–70 (1973).

[35]J. Chevalier, M. Saadaoui, C. Olagnon, and G. Fantozzi, "Double-Torsion Testing a 3Y-TZP Ceramic," *Ceram. Int.*, **22**, 171–77 (1996).

[36]M. Ciccotti, "Realistic Finite-Element Model for Double-Torsion Loading Configuration," *J. Am. Ceram. Soc.*, **83** [11] 2737–44 (2000).

[37]E. R. Fuller Jr., "An Evaluation of Double Torsion Testing– Analysis"; pp. 3–19 in Proceedings of the 11th Symposium of Fracture Mechanics: Part II, ASTM STP 678, *Fracture Mechanics Applied to Brittle Materials*. Edited by S. W. Freiman. American Society for Testing and Materials, Philadelphia, PA, 1979.

[38]B. J. Plekta, E. R. Fuller, and B. G. Koepke, "An Evaluation of Double Torsion Testing–Experimental"; *ibid*, pp. 19–38.

[39]M. E. Ebrahimi, J. Chevalier, and G. Fantozzi, "Slow Crack Growth of Alumina Ceramics," *J. Mater. Res.*, **15**, 142–47 (2000).

[40]J. Chevalier, "Slow Crack Growth Behavior of 3Y-TZP Biomedical Ceramics" (in Fr.); Ph.D. Thesis. National Institute of Applied Sciences of Lyon, Lyon, France, 1996.

[41]J. Chevalier, C. Olagnon, and G. Fantozzi, "Subcritical Crack Propagation in 3Y-TZP Ceramics: Static and Cyclic Fatigue," *J. Am. Ceram. Soc.*, **82** [11] 3129–38 (1999).

[42]B. Lawn, *Fracture of Brittle Solids*, 2nd Ed., Cambridge Solid State Science Series; p. 378. Cambridge University Press, Oxford, U.K., 1993.

[43]J. Chevalier, C. Olagnon, and G. Fantozzi, "Crack Propagation and Fatigue in Zirconia-Based Composites," *Composites (Guildford UK)*, Part A, 30, 525–30 (1999).

[44]G. Willmann, "Ceramic Femoral Heads for Total Hip Arthroplasty," *Adv. Eng. Mater.*, **2** [3] 114–22 (2000). □